Journal of Materials Chemistry C

ROYAL SOCIETY OF CHEMISTRY

PAPER

View Article Online
View Journal | View Issue

Cite this: J. Mater. Chem. C, 2025, 13, 3902

The role of fluorine substituents in the formation of the ferroelectric nematic phase†

Ewan Cruickshank, ‡*[a] Rebecca Walker, [a] Grant J. Strachan, [b] Ewa Górecka, [b] Damian Pociecha, [b] John M. D. Storey [a] and Corrie T. Imrie [a]

Received 2nd August 2024,
Accepted 20th December 2024

DOI: 10.1039/d4tc03318c

rsc.li/materials-c

The synthesis and characterisation of a group of molecules based on the skeletal structures of 4-[(4-nitrophenoxy)carbonyl]phenyl 4-methoxybenzoate and (4-nitrophenyl)-2-methoxy-4-(4-methoxybenzoyl)oxybenzoate is reported. Fluorine substituents are added to these structures and their liquid crystalline behaviour is characterised. All eight compounds reported exhibit the ferroelectric nematic phase, N_F, and in four of them the antiferroelectric phase labelled N_X is observed. These include rare examples of enantiotropic N_F and N_X phases, and several examples of the direct N_F-isotropic transition. The addition of a fluorine substituent reduces the nematic–isotropic transition temperature, and this is attributed to the reduction in both shape anisotropy and the ability of the molecules to form antiparallel dimers. The effect of the fluorine substituents on the N_F and N_X phases is less regular and interpreted in terms of the changes to the molecular shape and electron distribution. The stability of the N_X phase follows that of the N_F phase in the series without a lateral methoxy group. The addition of a lateral methoxy group reduces the stability of the N_F phase and completely suppresses the N_X phase.

Introduction

Following the experimental discovery of a polar nematic phase in 2017[1,2] and its subsequent assignment in 2020 as the ferroelectric nematic phase, N_F,[3] it has rapidly become the hottest topic in liquid crystal science and technology, not least due to its huge application potential. The N_F phase shows very large polarisation values, strong non-linear optical responses and giant dielectric permittivity values compared to those observed for the conventional nematic, N, phase.[4–30] We do note, however, that some doubt has been cast on these very large permittivity values by, for example, Erkoreka *et al.*[31] and Clark *et al.*[32] The phase also exhibits other interesting behaviour such as the formation of twisted structures in antiparallel rubbed cells.[33] Critically it is the polar nature of the N_F phase that gives rise to its fascinating fundamental behaviour and technologically valuable properties. The conventional N phase presently underpins liquid crystal display technologies[34] and is the least ordered liquid crystal phase. In the N phase, the molecules show long-range orientational ordering in the absence of long-range positional ordering. Thus, the rod-like molecules align along a common direction known as the director, which is represented by the unit vector, **n**. The N phase possesses inversion symmetry such that $\mathbf{n} = -\mathbf{n}$, Fig. 1, and hence is non-polar. By comparison, in the N_F phase, this inversion symmetry is broken such that $\mathbf{n} \neq -\mathbf{n}$, Fig. 1, and the phase is polar.

The overwhelming majority of approximately 200 molecules that have been reported to exhibit the N_F phase can be broadly grouped into one of two molecular templates, RM734 and DIO,

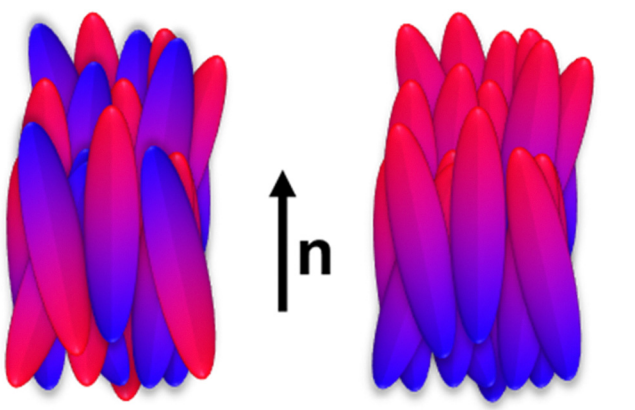

Fig. 1 Schematic representation of the conventional nematic phase (left) and the ferroelectric nematic phase (right).

[a] Department of Chemistry, University of Aberdeen, Old Aberdeen, AB24 3UE, UK. E-mail: e.cruickshank2@rgu.ac.uk
[b] Faculty of Chemistry, University of Warsaw, Zwirki i Wigury 101, 02-089 Warsaw, Poland

† Electronic supplementary information (ESI) available. See DOI: https://doi.org/10.1039/d4tc03318c

‡ Present address: School of Pharmacy, Applied Sciences and Public Health, Robert Gordon University, Aberdeen, AB10 7GJ, UK.

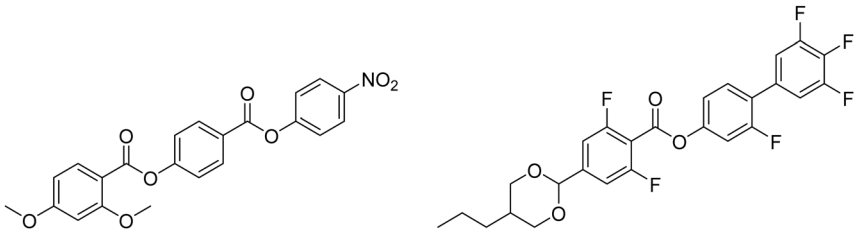

Fig. 2 Molecular structures of RM734 (left panel) and DIO (right panel).

Fig. 2.[6–8,11,13,17,18,20,26,30,35–55] These were the first compounds reported to exhibit the N_F phase[2,42] and although they appear rather chemically different, both possess a large longitudinal dipole moment and structural elements promoting lateral bulk. It has become apparent that the ester links in these structures play an important role in the formation of the N_F phase by disrupting the electronic distribution along the molecule such that it may be described as alternating regions of positive and negative charge density as sketched in Fig. 3.[56] This representation of the electron density is similar to the longitudinal charge density waves used by Madhusudana to describe molecules and account for the formation of the N_F phase.[57] Specifically, the model suggests that the parallel alignment of the molecules is enhanced by minimising the amplitude of the charge density wave at either end of the molecule. Molecular dynamics simulations reported by Mandle also reveal that the molecules are displaced along their long axes to allow the favourable overlap of negative and positive regions in a parallel orientation.[58,59] We recently highlighted the challenge in generating more exotic structures within this structure space through the design of highly polar dimers which, despite appearing to have the features described earlier, did not exhibit the N_F phase.[60]

We have previously reported on the role played by fluorine substituents in RM734-type compounds in the formation of the N_F phase, focussing our attention on fluorine substituents on the middle aromatic ring and in the *ortho* position to the terminal nitro group.[8,20,26,36,46,51] Here we extend our study and consider the effects on the N_F phase of fluorine substituents on the 4-methoxybenzoic acid fragment. This work will look to expand on the fluorinated materials reported by Li *et al.*[6] and this will be undertaken by adding fluorine atoms next to the terminal nitro group and removing the lateral methoxy group in the middle aromatic ring. We recently reported that adding methoxy groups to the middle aromatic ring of RM734-type compounds decreased the value of the N_F transition temperatures and extinguished the conventional nematic phase. Therefore, we would expect the compounds we are reporting herein, in which the methoxy group is removed from the middle aromatic ring, to show a stabilisation of the N_F phase. Here we report the synthesis and characterisation of eight compounds structurally related to RM734 each containing fluorine substituents on the 4-methoxybenzoic acid fragment rather than a lateral methoxy group and designed to exhibit the N_F phase. We refer to these compounds using the code EC*n*F and their structures are shown in Table 1. Of these eight compounds, six are reported here for the first time. The properties of these compounds will allow us to better understand the structural factors that drive the formation of the fascinating N_F phase which in turn will underpin the rational design of new materials having targeted properties.

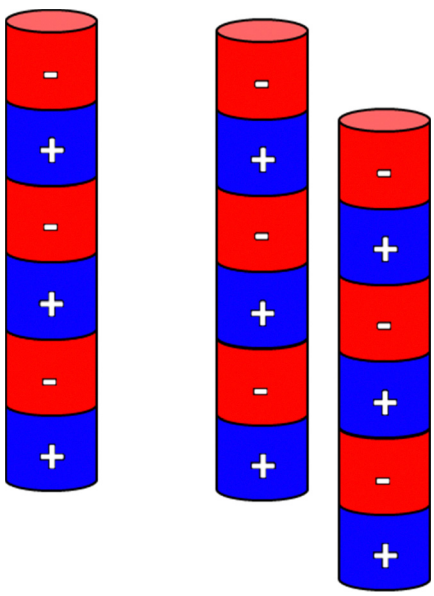

Fig. 3 Sketch of a rod-like molecule with regions of positive and negative charge (left) and the favoured parallel alignment of rods in the N_F phase (right).

Experimental

The synthetic route used to prepare **EC1F**, **EC2F**, **EC5F** and **EC6F** is shown in Scheme 1 and for **EC3F**, **EC4F**, **EC7F** and **EC8F** in Scheme 2. A detailed description of the preparation of the intermediates and final products, including their structural characterisation, is provided in the ESI.†

Optical studies

Phase characterisation was performed using polarised light microscopy, using a Zeiss AxioImager A2m equipped with a Linkam THMS600 hot stage. Slides treated for planar alignment were purchased from INSTEC or AWAT with a thickness between 2.9–3.5 μm or 1.8 μm, respectively, and both sets of cells were ITO conducting.

Differential scanning calorimetry

The phase behaviour of the materials was studied by differential scanning calorimetry performed using a Mettler Toledo DSC1 or DSC3 differential scanning calorimeter equipped with

Table 1 Structures of the target compounds and the codes used to refer to them

Code	Structure	Code	Structure
EC1F	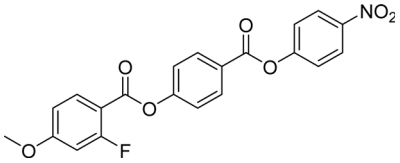	**EC2F**	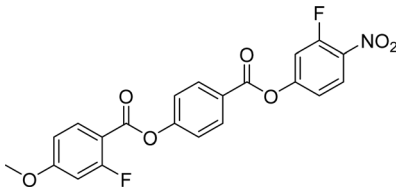
EC3F	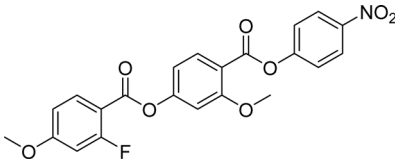	**EC4F**	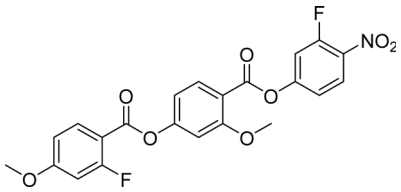
EC5F	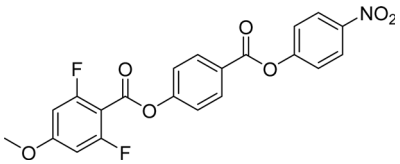	**EC6F**	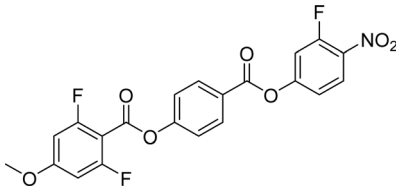
EC7F	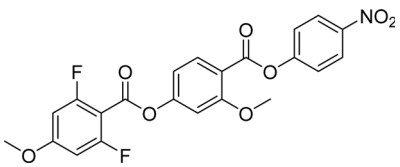	**EC8F**	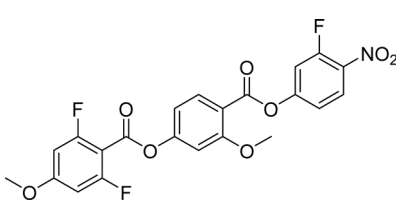

TSO 801RO sample robots and calibrated using indium and zinc standards. Heating and cooling rates were 10 K min^{-1}, with a 3 min isotherm between either heating or cooling, and all samples were measured under a nitrogen atmosphere. Transition temperatures and associated enthalpy changes were extracted from the heating traces unless otherwise noted. For each sample, two aliquots were measured, and the data listed are the average of the two sets of data.

Molecular modelling

The geometric parameters of the compounds of interest were obtained using quantum mechanical DFT calculations with Gaussian09 software.[61] Optimisation of the molecular structures was carried out at the B3LYP/6-31G(d) level. Visualisations of electronic surfaces and ball-and-stick models were generated from the optimised geometries using the GaussView 5 software. The electronic surfaces were found using the cubegen utility in GaussView by generating a total density cube using a SCF density matrix and coarse grid, overlayed by an ESP surface map. Visualisations of the space-filling models were produced post-optimisation using the QuteMol package.[62]

Birefringence measurements

Birefringence was measured with a setup based on a photoelastic modulator (PEM-90, Hinds) working at a modulation frequency f = 50 kHz; as a light source, a halogen lamp (Hamamatsu LC8) was used equipped with narrow bandpass filter (532 nm). The signal from a photodiode (FLC Electronics PIN-20) was deconvoluted with a lock-in amplifier (EG&G 7265) into 1f and 2f components to yield a retardation induced by the sample. Knowing the sample thickness, the retardation was recalculated into optical birefringence. Samples were prepared in 3.0 μm-thick cells with planar anchoring. The alignment quality was checked prior to measurement by inspection under the polarised light optical microscope.

Dielectric spectroscopy

The complex dielectric permittivity, ε^*, was studied using a Solartron 1260 impedance analyser. Measurements were conducted in the 10 Hz–1 MHz frequency (f) range, with the probe voltage of 20 mV, and it was checked by optical observations that such a voltage is below the Fredericks transition threshold. The material was placed in 9.7 μm-thick glass cells with gold electrodes and no polymer aligning layers. Regardless of the way the dielectric spectroscopy results are interpreted, when a material with a giant permittivity is tested, instead of charging, and thus measuring the capacitor with the LC sample only the surface layers are charged because they have a smaller capacitance even though they are much thinner. Hence cells without polymer aligning layers were used in order to help this somewhat. The lack of a surfactant layer resulted in the random configuration of the director in the liquid crystal phases; microscopic observations of the optical textures suggested a dominant planar orientation without the preferable direction of the long molecular axis.

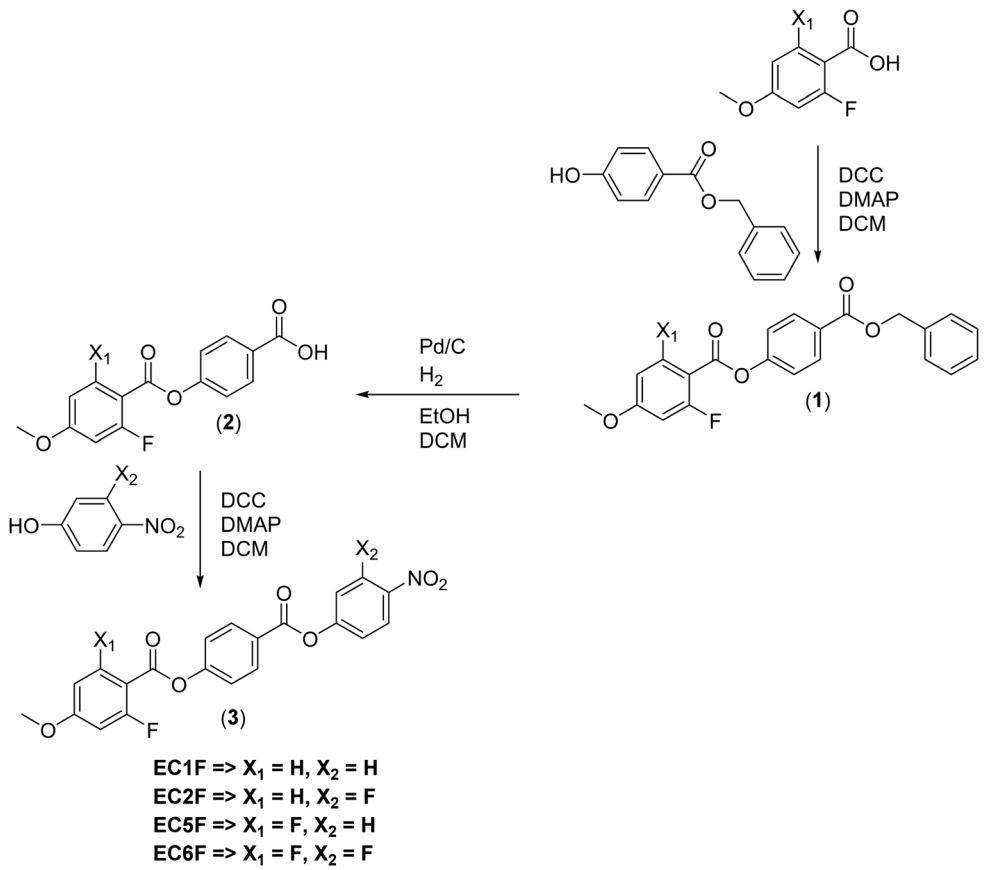

Scheme 1 Synthetic route used to prepare **EC1F**, **EC2F**, **EC5F** and **EC6F**.

Second harmonic generation

The SHG activity was tested using a microscopic setup. Solid-state laser EKSPLA NL202 pulses (λ = 1064 nm, 9 ns, 10 Hz repetition rate and max. 2 mJ pulse energy) were incident onto a LC sample prepared in 10 μm-thick glass cells with planar anchoring condition. An IR pass filter was placed at the entrance to the sample and a green pass filter at the exit of the sample.

X-ray diffraction

The X-ray diffraction (XRD) measurements were performed with a Bruker D8 GADDS system (CuKα line, Goebel mirror monochromator, point beam collimator, Vantec2000 area detector). The temperature of the sample was controlled with a precision of ±0.1 K. Samples were prepared as droplets on a heated surface.

Results and discussion

The transitional properties of the EC*n*F compounds (Table 1) are listed in Table 2. The transition temperatures of **EC3F** and **EC7F** are in good agreement with those reported previously by Li *et al.*[6] Five of these compounds, specifically **EC1F**, **EC2F**, **EC3F**, **EC5F** and **EC6F**, exhibited the conventional nematic (N) phase and this was assigned on the observation of characteristic textures. Thus, for samples sandwiched between untreated glass slides a schlieren texture containing two- and four-brush point singularities was observed (Fig. 4(a)) which flashed when subjected to mechanical stress, and for samples in cells treated for planar alignment, a uniform texture was seen (Fig. 4(b)). On cooling the N phase shown by **EC2F**, **EC5F** and **EC6F**, a chevron texture developed indicative of the N_X phase (Fig. 4(c) and (d)).[8,44,47,51,63] The N_X phase is also referred to as the SmZ_A phase and consists of a regular array of polar domains arranged in an anti-ferroelectric fashion along the direction perpendicular to the director.[44,53,63–65] This question of nomenclature for this phase is yet to be resolved as there is a sharp XRD signal sometimes recorded in this phase, corresponding to the periodic domain structure, which would be considered a feature of a smectic phase. Simultaneously, a diffuse XRD signal is always observed reflecting liquid-like positional correlations for neighbouring molecules, suggesting a more nematic nature to the phase.[47]

On cooling the chevron texture of the N_X phase seen for **EC2F**, **EC5F** and **EC6F**, a highly birefringent, banded texture (Fig. 4(e)) or a texture showing twisted states (Fig. 4(f)) formed, characteristic of the formation of the N_F phase.[14,20,30,36,41,51] A similar banded texture was seen on cooling the schlieren texture of the N phase of **EC3F** indicating a N_F–N transition, and was also observed directly from the isotropic phase for **EC4F**, **EC7F** and **EC8F** implying a N_F-I transition. The domains apparent in these banded textures (Fig. 4(e)) are areas in which

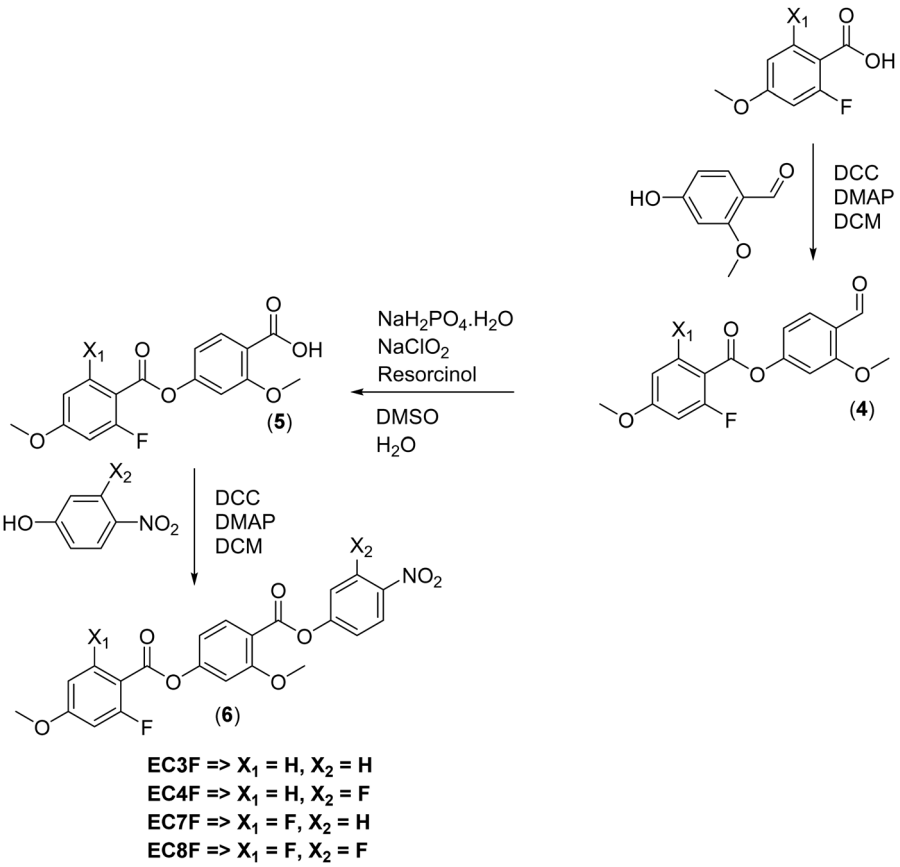

Scheme 2 Synthetic route used to prepare **EC3F**, **EC4F**, **EC7F** and **EC8F**.

the director has differing orientations and thus the orientation of the polarisation also differs and appears to be 'banded' due to the differing areas of birefringence within the domains.

Table 2 Transition temperatures (in °C) and associated entropy changes scaled by the gas constant (values in parentheses) for the EC*n*F compounds (for structures see Table 1). The transitions are listed on heating (top) and cooling (bottom). The enthalpies of crystallisation on cooling are not listed. The calculated dipole moment, μ, is also included

Name	Phase sequence	μ/D
EC1F	Cr-207 (11.8)-N-278 (0.13)-I	10.98
	I-276[a]-N-157[a]-N_X-144[a]-N_F-162[c]-Cr	
EC2F	Cr-192 (9.85)-N-245 (0.16)-I	12.02
	I-244 (0.18)-N-175 (0.003)-N_X-166 (0.12)-N_F-155-Cr	
EC3F	Cr-169 (12.4)-N-177 (0.16)-I	12.26
	I-176 (0.21)-N-156 (0.24)-N_F-141-Cr	
EC4F	Cr-172 (15.3)-I	13.31
	I-153 (1.25)-N_F-112-Cr	
EC5F	Cr-186 (9.87)-N-266[a]-I	11.18
	I-265[a]-N-177-N_X-172 (0.09[b])-N_F-134-Cr	
EC6F	Cr-181 (8.44)-N_F-188 (0.17[b])-N_X-191–231 (0.16)-I	12.16
	I-232 (0.16)-N-189-N_X-187 (0.22[b])-N_F-148-Cr	
EC7F	Cr-167 (13.6)-I	12.58
	I-159 (1.07)-N_F-110-Cr	
EC8F	Cr-162 (13.0)-I	13.64
	I-149 (1.44)-N_F-140-Cr	

[a] Measured using polarised light microscopy. [b] Represents a combined entropy change arising from overlapping peaks in the DSC trace. [c] Crystallisation temperature of sample bulk, mesophases observed in isolated droplets.

The proposed phase assignments are consistent with the values of the associated scaled entropy changes, $\Delta S/R$, listed in Table 2. The values of $\Delta S_{NI}/R$ range between 0.13 to 0.21, and these are lower than typically measured for a conventional low molar mass nematogen for which $\Delta S_{NI}/R \approx 0.3$. These smaller values presumably reflect the enhanced molecular biaxiality associated with the lateral substituents that reduce the orientational order of the nematic phase and hence, reduce $\Delta S_{NI}/R$.[66] The values of the scaled entropy change associated with the N_F-I transition, $\Delta S_{N_FI}/R$, are several times larger than $\Delta S_{NI}/R$ and this additional entropic contribution is associated with the ordering of the dipoles in the N_F phase.

On cooling the N phase shown by **EC1F**, crystallisation in the bulk precluded the observation of the characteristic textures for the N_F and N_X phases shown in Fig. 4. Instead, the N–N_X and N_X–N_F transitions were observed only for isolated droplets. To assign these phase transitions a phase diagram (Fig. 5) was constructed for binary mixtures of **EC1F** and the ferroelectric nematogen, **4EC6F** (Fig. 6).[47] The compounds were miscible over the entire composition range, and each mixture exhibited N, N_X and N_F phases assigned on the observation of characteristic optical textures (Fig. 7). Adding **EC1F** to **4EC6F** sees T_{NI}, T_{N_XN} and $T_{N_FN_X}$ increase in essentially a linear manner. Extrapolation of the trendlines provides estimates of the virtual transition temperatures for **EC1F** of T_{NI} = 266 °C, T_{N_XN} = 146 °C and $T_{N_FN_X}$ = 137 °C, with the values for the pure sample

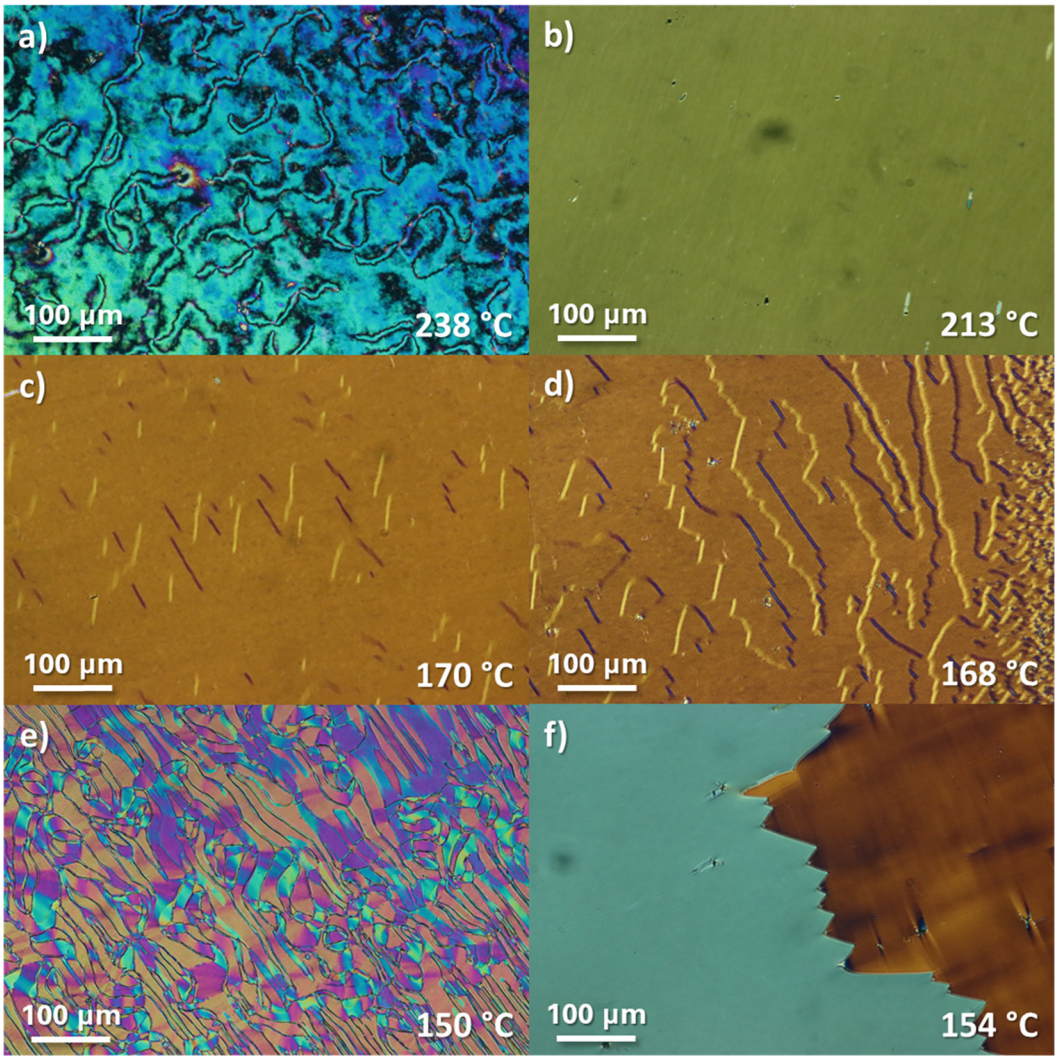

Fig. 4 Optical textures obtained for **EC2F** using polarised optical microscopy: (a) schlieren texture of the nematic phase seen for a sample sandwiched between untreated glass slides; the remaining textures were observed for samples in cells treated for planar anchoring, (b) uniform texture of the nematic phase, (c) and (d) chevron textures of the N_X phase, (e) banded texture of the ferroelectric nematic phase and (f) texture showing the twisted states of the ferroelectric nematic phase.

of **EC1F** not included. These values are slightly lower than the transition temperatures measured for isolated droplets of **EC1F** using polarised optical microscopy but strongly support the assignments listed in Table 1.

X-ray diffraction was used to characterise the N, N_X and N_F phases and representative diffraction patterns for **EC5F** are shown in Fig. 8. Only diffuse scattering is seen in these patterns arising from the short-range positional ordering of the molecules in all three phases. The periodic structure of the antiferroelectric domains in the N_X phase should give rise to a sharp reflection at small angles in the X-ray diffraction pattern. This signal has a very low intensity, however, showing that the related electron density modulation is particularly weak, and in practice, a strong synchrotron source is required for it to be observed.[47]

The temperature dependence of the optical birefringence, Δn, for **EC2F** is shown in Fig. 9. A particularly small change in Δn of just ≈ 0.01 is seen at the N–N_X transition indicating that the N_X phase is orientationally very similar to the conventional N phase. This is followed by a larger but still small step-like increase at the N_X–N_F transition indicative of an increase of the order parameter, S. These observations are in complete accord with our previous reports of the temperature dependence of the optical birefringence of the N_X and N_F phases.[47,51] The polar character of the nematic phases exhibited by **EC2F** was tested by measuring its complex permittivity as a function of temperature and frequency (Fig. 10). On cooling through the nematic phase, a weak dielectric mode begins to develop with a relaxation frequency slightly above 10^4 Hz, which shows typical softening due to the increasing polar order, with ε' increasing to *ca.* 100, while the frequency decreases approaching the N–N_X transition. On entering the N_X phase, this mode is quenched, most probably due to the antiferroelectric nature of this phase as we have previously reported.[47] The N_X–N_F

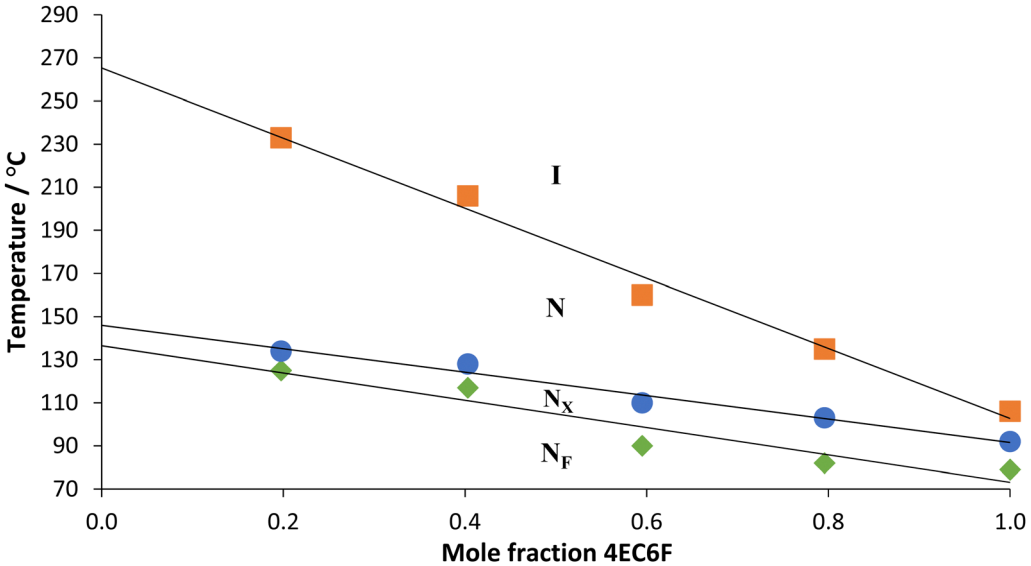

Fig. 5 Phase diagram constructed using binary mixtures of **EC1F** and **4EC6F**.[47] Squares denote T_{NI}, circles T_{N_XN} and triangles $T_{N_FN_X}$. The trendlines are shown for T_{NI}, T_{N_XN} and $T_{N_FN_X}$.

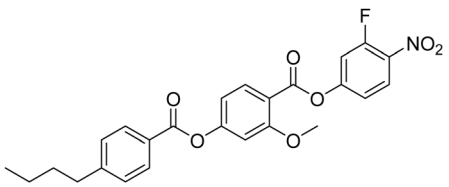

Fig. 6 Molecular structure of **4EC6F**.

transition is marked by the abrupt increase of the measured low-frequency permittivity, by orders of magnitude, which is characteristic of the N_F phase. While the proper detailed interpretation of the measured permittivity values in the N_F phase is more complex than previously thought, with many recent articles suggesting a variety of interpretations of what the values should be and why,[12,31,32,67–70] these considerations are beyond the scope of this paper which has a focus on the effect of structural modifications on the phase behaviour. However, the measured temperature dependence of permittivity can be treated as qualitative proof for the determined sequence of polar phases, as it is in excellent agreement with data reported for other ferroelectric nematogens.[6–12,14,30] The non-centrosymmetric nature of the N_F phase in compound **EC2F** has been also confirmed by observation of its SHG activity. Incident IR (λ = 1064 nm) radiation resulted in a strong emission of green light (Fig. 10c), proving the ferroelectric ground state of the phase.

We now turn our attention to discuss the transition temperatures listed in Table 2 and how these relate to changes in molecular structure with a particular focus on the role played by fluorine substituents in driving the formation of the N_F phase. With this in mind, the eight compounds listed in Table 2 may be split into two groups of four depending whether they are based on 4-[(4-nitrophenoxy)carbonyl]phenyl 4-methoxybenzoate (**11-0-1**)[46] or (4-nitrophenyl)2-methoxy-4-(4-methoxybenzoyl)oxybenzoate (**NT3.1**).[20] The structures and transition temperatures of **11-0-1** and **NT3.1** are shown in Fig. 11. **11-0-1** has no lateral substituents and exhibits exclusively conventional N behaviour whereas **NT3.1** possesses a lateral methoxy substituent on the central ring and shows both N_F and N phases. We note that isolated droplets of the N phase shown by **11-0-1** may be supercooled to 107 °C prior to crystallisation but attempts to measure a virtual N_F–N transition temperature were not successful.[46] The addition of a fluorine substituent *ortho* to the nitro group in **11-0-1** gives **12-0-1** and this is also exclusively nematic, see Fig. 11.

Fig. 12 maps the changes in the three transition temperatures, T_{NI}, T_{N_XN} and $T_{N_FN_X}$, on increasing the number of fluorine substituents from the unsubstituted **11-0-1** to **EC6F** containing three fluorine atoms. **EC6F** is a particularly interesting compound as it exhibits enantiotropic N_X and N_F phases. The addition of a fluorine atom always reduces T_{NI} but the magnitude of this decrease depends on the resulting change in structure. Thus, adding the first fluorine atom to the methoxyphenyl ring reduces T_{NI} by around 6 K, and the second by about 13 K, irrespective of whether the nitrophenyl ring contains a fluorine atom or not. The addition of the fluorine atom *ortho* to the nitro group reduces T_{NI} by about 33 K irrespective of the number of fluorine atoms on the methoxyphenyl ring. By contrast, adding fluorine atoms always increases both T_{N_XN} and $T_{N_FN_X}$ with the exception of moving from **11-0-1** to **12-0-1** for which N_X and N_F phases are not observed. It is clear, however, that $T_{N_FN_X}$ and T_{N_XN} must both be higher for **EC1F** than **12-0-1** by at least 44 K and 57 K, respectively, indicating that a fluorine atom *ortho* to the methoxy group is considerably more effective in promoting the N_F and N_X phases than if *ortho* to the nitro group. This is also evident in the dramatic increase in $T_{N_FN_X}$ and T_{N_XN} passing from **12-0-1** to **EC2F** of at least 66 K and 75 K,

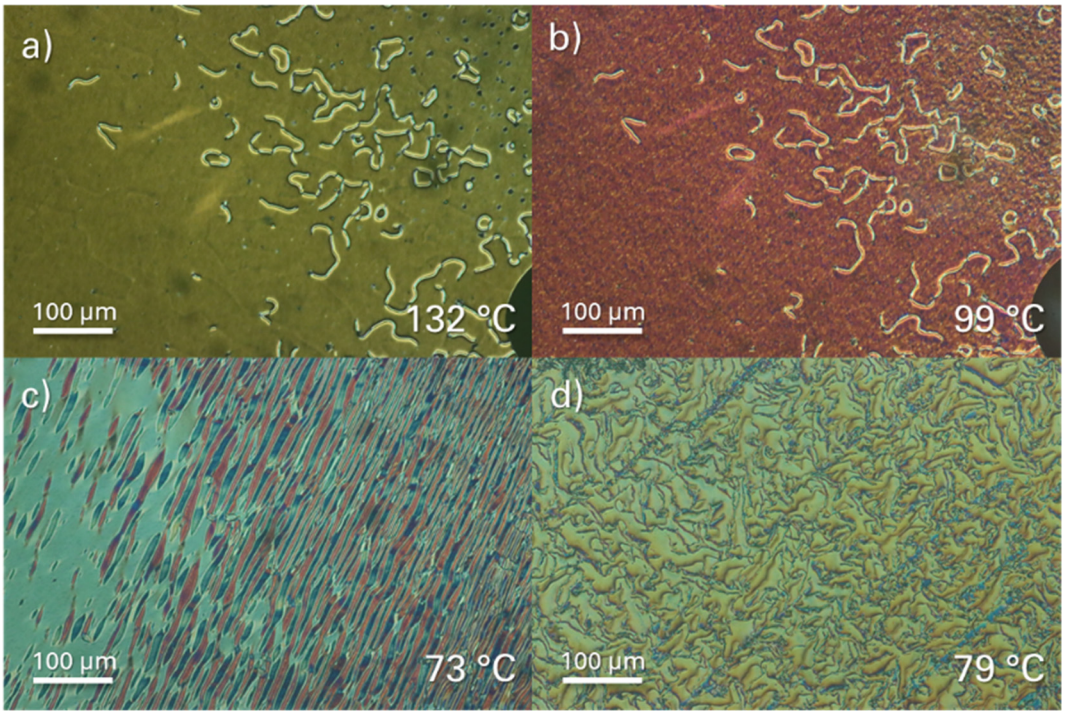

Fig. 7 Optical textures obtained using polarised light microscopy for a binary mixture composed of 40 mol% **EC2F** and 60 mol% **4EC6F** contained in a cell treated for planar alignment in (a) the N, (b) the N_X, and (c) the N_F phase. (d) The texture of the N_F phase obtained for a sample sandwiched between untreated glass slides.

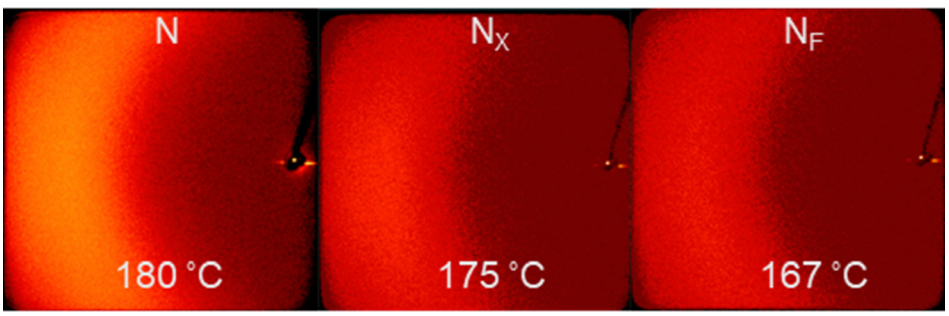

Fig. 8 X-ray diffraction patterns obtained for **EC5F** in (left) the N, (middle) N_X and (right) N_F phases.

respectively. After the addition of the first fluorine atom to the methoxyphenyl ring, subsequent fluorine atoms have a much smaller effect, and it appears to make little difference in which order they are added. This culminates in the compound **EC6F** which contains three fluorines within the molecular structure and exhibits both enantiotropic N_X and N_F phases.

Fig. 13 shows the changes in $T_{N_FN/I}$ and T_{NI} on increasing the number of fluorine atoms from the unsubstituted **NT3.1** to **EC8F** containing three fluorine atoms. Again, it is evident that the addition of a fluorine atom always decreases T_{NI}. Broadly the trends are the same as described for the **11-0-1**-based materials. The largest decreases in T_{NI} are observed on adding a fluorine atom *ortho* to the nitro group. The reduction in T_{NI} associated with the addition of the fluorine atoms is sufficiently large for the nematic phase to be extinguished and a direct N_F-I transition to be observed for three of the four **NT3.1**-based compounds. The effect of adding a fluorine atom on $T_{N_FN/I}$ is smaller than seen for the **11-0-1**-based materials and depending on the structure may be positive or negative, which agrees with our recently published work on other ferroelectric nematic materials.[46]

We have seen that the addition of a fluorine atom to a compound in this collection always leads to a decrease in T_{NI} and this effect is most pronounced when the fluorine atom is *ortho* to the nitro group. This reflects, at least in part, the reduction in structural anisotropy arising from the lateral substituent, see Fig. 14, and this is most pronounced for a fluorine atom *ortho* to the nitro group (Fig. 14(d)). This alone, however, cannot account for the observed trends given that these are similar for both sets of materials even though the

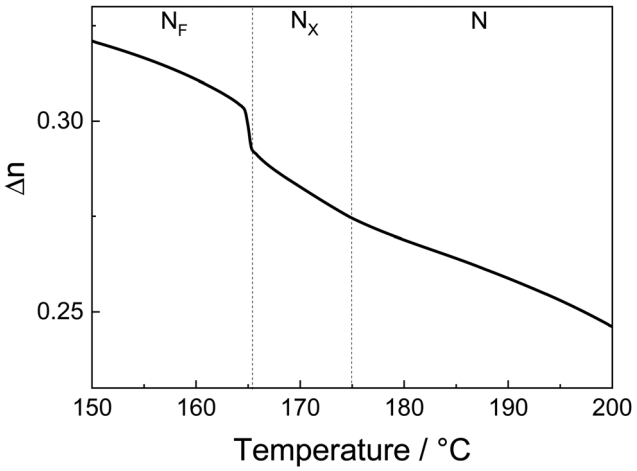

Fig. 9 Temperature dependence of the optical birefringence of **EC2F** measured on cooling with green light (λ = 532 nm).

relative change in shape will be smaller for the **NT3.1**-based materials (Fig. 14(c)). This suggests that the fluorine atom *ortho* to the nitro group inhibits the antiparallel association of these molecules and this will also reduce T_{NI}. This accounts for the smaller reductions in T_{NI} seen for additions of fluorine atoms to the methoxyphenyl ring as these will have a much smaller effect on the antiparallel association of the molecules. In addition, the effect on shape of the first fluorine atom added to the methoxyphenyl ring is reduced by the molecular structure (Fig. 14(a)). By comparison, the second fluorine atom protrudes from the excluded molecular volume (Fig. 14(b)) and gives rise to a larger reduction in T_{NI} than seen for the first fluorine atom.

Our previous studies have suggested that a combination of electronic and shape factors drive the formation of the N_F phase[20,41,46] and even less is presently understood about the N_X phase.[47,51] For the **11-0-1**-based materials a fluorine atom on the methoxyphenyl ring strongly promotes both N_F and N_X phases, whereas a single fluorine atom *ortho* to the nitro group does not. We have already noted that the change in shape arising from the addition of the first fluorine atom to the methoxyphenyl ring must be small given the associated weak change in T_{NI}, and hence, the effect on the N_F and N_X phases must arise from the change in the electron distribution. The addition of the fluorine atom reduces the electron density associated with the methoxyphenyl ring (Fig. 14(a)). Within the framework of the model proposed by Madhusudana to account for the formation of the N_F phase[57] described earlier, minimising the amplitude of the charge density wave at either end of the molecule reduces the tendency to adopt anti-parallel structures and the N_F phase is stabilised. The second fluorine atom further reduces the charge density associated with the methoxyphenyl ring and also enhances the molecular biaxiality (Fig. 14(b)) further promoting the N_F and N_X phases. The single fluorine atom *ortho* to the nitro group in **12-0-1** in itself does not promote the formation of the N_F phase because the molecule does not favourably pack into parallel structures presumably due to its shape. This is despite the fluorine atom reducing the amplitude of the charge density wave at the end of the molecule and is indicative that the position of lateral substituents is a critical consideration in the phase behaviour of these materials. The shape requirement for observing the N_F phase is satisfied by the addition of fluorine atoms to the methoxyphenyl ring, and the combination of the three fluorine atoms gives rise to the highest values of $T_{N_FN_X}$ and T_{N_XN}.

The effects of the fluorine atoms on the N_F phases shown by the **NT3.1**-based materials are smaller than seen for the **11-0-1**-based compounds and may either increase or decrease the transition temperatures. This cannot be accounted for entirely using Madhusudana's model, which would predict similar behaviour for both sets of compounds.[57] This presumably reflects the weaker change in shape arising from the addition of the fluorine atoms in the case of the **NT3.1**-based compounds and suggests that some optimum molecular shape exists for the observation of the N_F phase. The presence of both the methoxy and fluorine substituents may exceed this shape constraint and overcome the electronic contributions the fluorine atoms play in the formation of the N_F such that a decrease in $T_{N_FN/I}$ is observed.

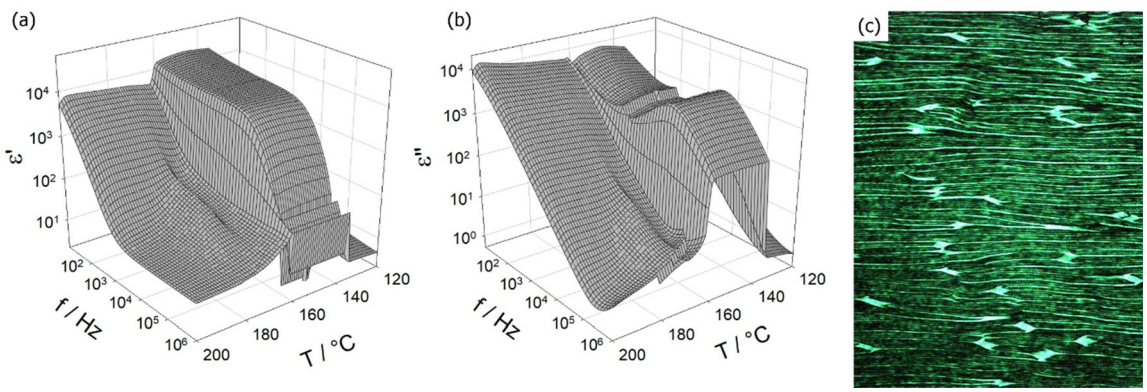

Fig. 10 (a) Real and (b) imaginary parts of the complex dielectric permittivity measured as a function of temperature and frequency for **EC2F**. (c) Image taken with an SHG microscope in the ground state (no applied voltage) N_F phase (at 155 °C) for a sample prepared in a cell with planar anchoring. Incident IR radiation caused strong emission of double-frequency (green) light.

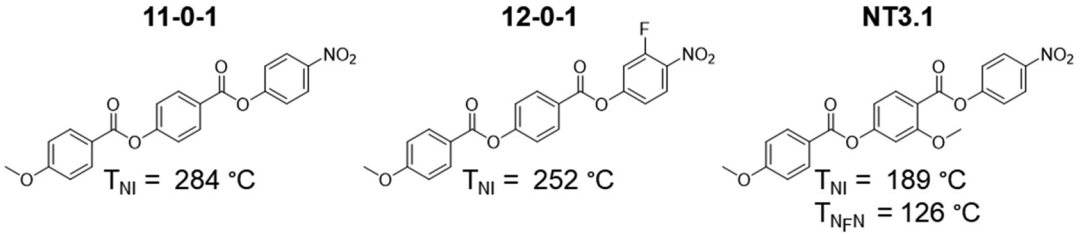

Fig. 11 Structures and transition temperatures of **11-0-1** and **12-0-1**[46] and **NT3.1**.[20]

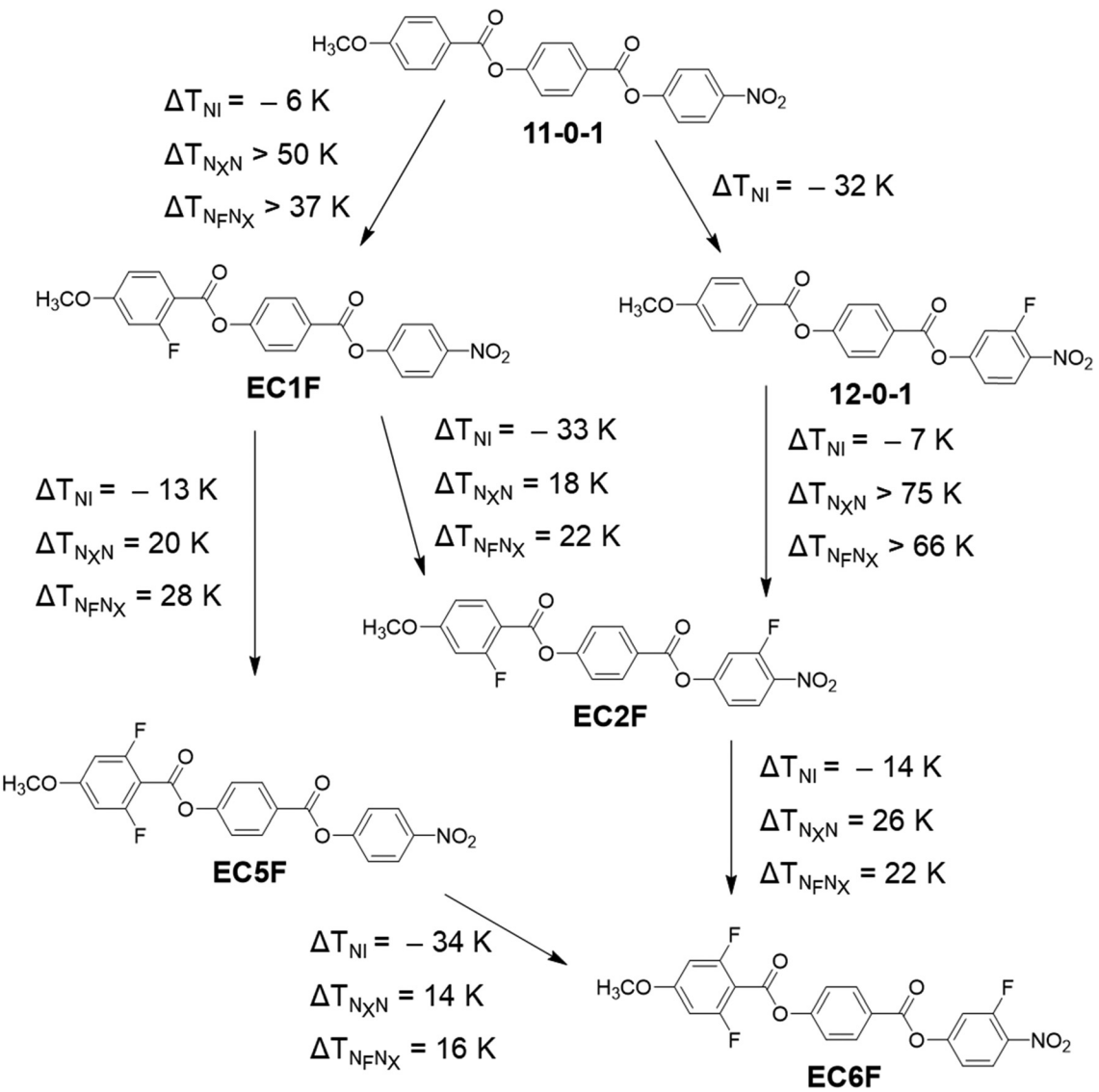

Fig. 12 The differences in transition temperatures between compounds based on **11-0-1**.

Finally, we will consider the role of the methoxy lateral group and compare these two sets of molecules. As would be expected on the basis of shape, the addition of the lateral methoxy group reduces T_{NI} by around 95 K. The smallest reduction, 82 K, is for the pair of molecules containing the highest number of fluorine substituents, **EC6F** and **EC8F**, and this reflects the smaller relative change in shape associated with the methoxy group. As we have seen, neither **11-0-1** nor **12-0-1** exhibit the N_F phase and the addition of the lateral methoxy group to the central phenyl ring has a pronounced effect, increasing T_{N_FN} by at least 19 K and 42 K, respectively. The situation is more difficult to establish for the remaining pairs of

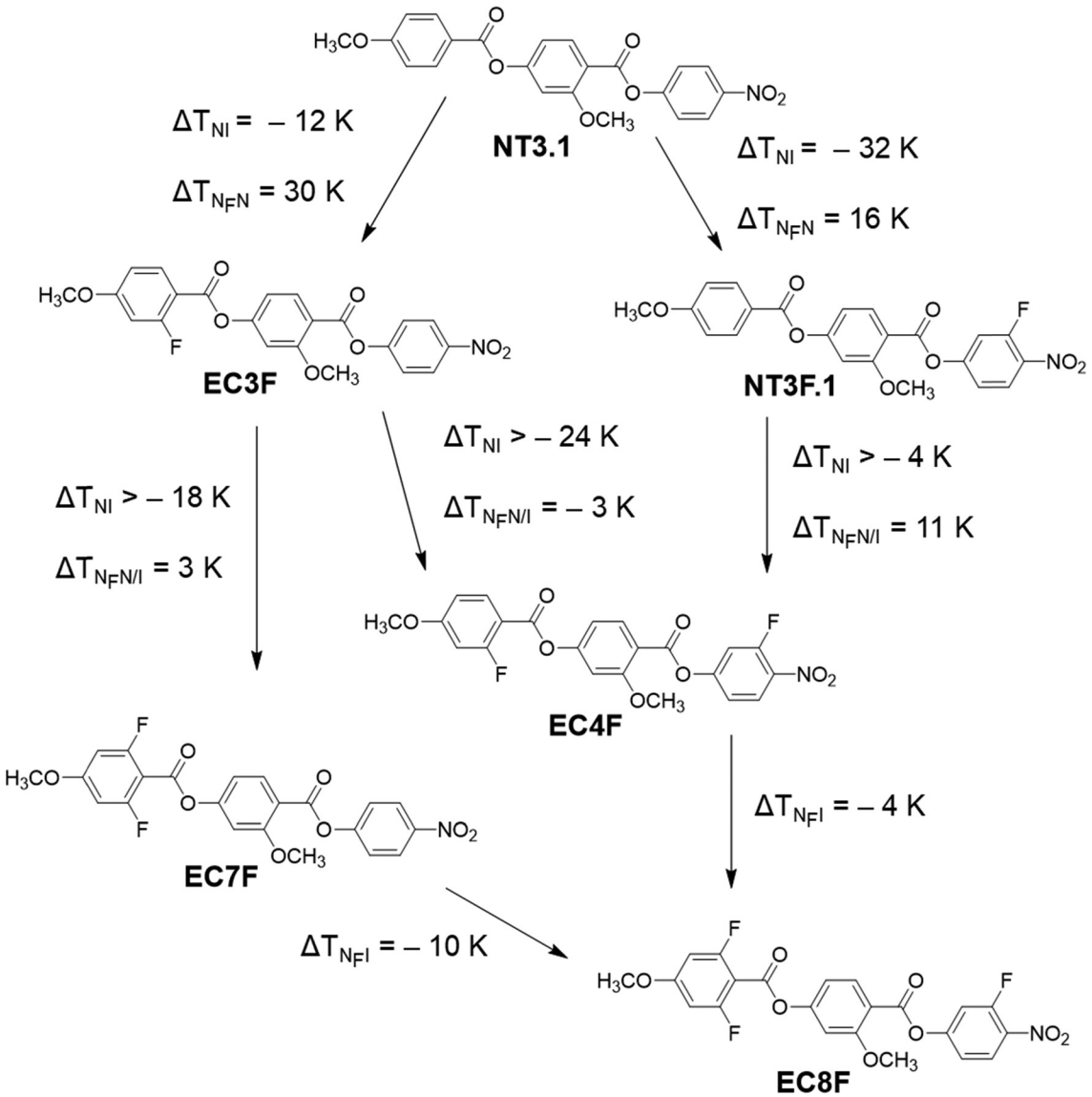

Fig. 13 The differences in transition temperatures between compounds based on **NT3.1**.

compounds because differing phase transitions are being compared. It is clear, however, that for three of the pairs, **EC2F**/**EC4F**, **EC5F**/**EC7F** and **EC6F** (which has an enantiotropic N_F-I transition)/**EC8F**, the stability of the N_F phase is reduced on the

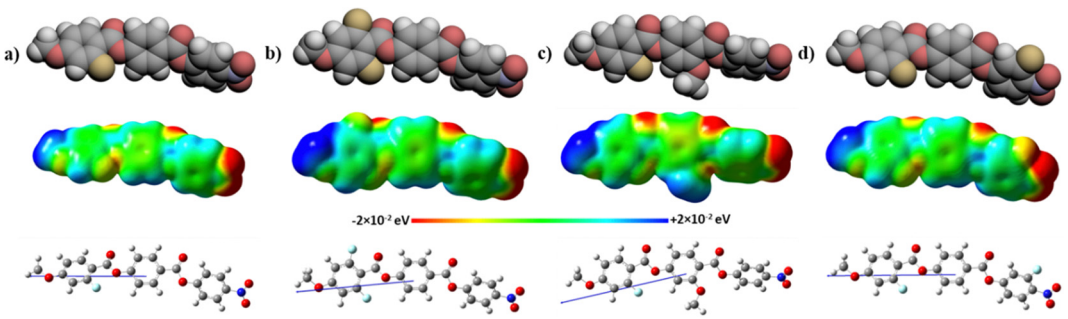

Fig. 14 The space-filling models (top), electrostatic potential surfaces (middle) and ball-and-stick models (bottom) of (a) **EC1F**, (b) **EC5F**, (c) **EC3F** and (d) **EC2F** calculated at the B3LYP/6-31(d) level of theory. The arrow indicates the direction of the calculated dipole moment, with the head representing the positive charge moving to the base which is negative.

addition of the methoxy group and for the fourth, **EC1F**/**EC3F**, there appears little change. Certainly, the addition of the methoxy group will increase the amplitude of the charge density wave in the centre of the molecule and this will promote the formation of the N_F phase and hence the observed increase in transition temperatures for the **11-0-1**/**NT3.1** and **12-0-1**/**NT3F.1** pairs of molecules. Presumably for the remaining pairs, shape considerations must account for the reduced tendency to exhibit the N_F phase for the methoxy-substituted materials. It is interesting to note that the methoxy substituent in the middle aromatic ring has suppressed the formation of the N_X phase and the physical significance of this requires further investigation.

Conclusions

We report two sets of new ferroelectric nematogens to investigate the role played by fluorine substituents on the formation of the N_F phase. The addition of fluorine substituents reduces T_{NI}. The magnitude of this decrease depends on the position of the fluorine atom, and this is interpreted in terms of its effect on molecular shape and the tendency of the molecules to form antiparallel dimers. The effect of fluorine substituents on the stability of the N_F phase is more strongly dependent on the molecular structure and $T_{N_FN/I}$ may increase or decrease. This is interpreted in terms of a competition between changes to molecular shape and electron distribution. It appears that there is some optimum shape for the formation of the N_F phase and if the addition of lateral substituents enhances the biaxiality beyond this, then the tendency to exhibit the N_F phase is reduced. The contributions of the electronic effects are well accounted for in terms of the model proposed by Madhusudana.[57] It is interesting to note that the stability of the N_X phase with respect to changes in the molecular structure appears similar to that of the N_F phase for the **11-0-1**-based materials and these materials provide a rare opportunity to study this. By contrast, the addition of a lateral methoxy group extinguishes the N_X phase. The physical significance of this observation is far from clear. In terms of the molecular engineering of materials, fluorine substituents clearly have an important role to play in the design of ferroelectric nematogens and here we report a rare example of a single compound exhibiting both enantiotropic N_F and N_X phases.

Data availability

The data supporting this article have been included as part of the ESI.†

Conflicts of interest

There are no conflicts to declare.

Acknowledgements

C. T. I. and J. M. D. S. acknowledge the financial support from the Engineering and Physical Sciences Research Council [EP/V048775/1]. The research was also supported by the National Science Centre (Poland) under the grant no. [2021/43/B/ST5/00240]. The authors thank Dr Jadwiga Szydłowska for their help in performing the SHG experiment.

References

1 R. J. Mandle, S. J. Cowling and J. W. Goodby, A nematic to nematic transformation exhibited by a rod-like liquid crystal, *Phys. Chem. Chem. Phys.*, 2017, **19**, 11429–11435.
2 H. Nishikawa, K. Shiroshita, H. Higuchi, Y. Okumura, Y. Haseba, S. I. Yamamoto, K. Sago and H. Kikuchi, A Fluid Liquid-Crystal Material with Highly Polar Order, *Adv. Mater.*, 2017, **29**, 1702354.
3 X. Chen, E. Korblova, D. Dong, X. Wei, R. Shao, L. Radzihovsky, M. A. Glaser, J. E. Maclennan, D. Bedrov, D. M. Walba and N. A. Clark, First-principles experimental demonstration of ferroelectricity in a thermotropic nematic liquid crystal: polar domains and striking electro-optics, *Proc. Natl. Acad. Sci. U. S. A.*, 2020, **117**, 14021–14031.
4 F. Caimi, G. Nava, R. Barboza, N. A. Clark, E. Korblova, D. M. Walba, T. Bellini and L. Lucchetti, Surface alignment of ferroelectric nematic liquid crystals, *Soft Matter*, 2021, **17**, 8130–8139.
5 P. Rudquist, Revealing the polar nature of a ferroelectric nematic by means of circular alignment, *Sci. Rep.*, 2021, **11**, 24411.
6 J. Li, Z. Wang, M. Deng, Y. Zhu, X. Zhang, R. Xia, Y. Song, Y. Hisai, S. Aya and M. Huang, General phase-structure relationship in polar rod-shaped liquid crystals: importance of shape anisotropy and dipolar strength, *Giant.*, 2022, **11**, 100109.
7 R. Saha, P. Nepal, C. Feng, M. S. Hossain, M. Fukuto, R. Li, J. T. Gleeson, S. Sprunt, R. J. Twieg and A. Jákli, Multiple ferroelectric nematic phases of a highly polar liquid crystal compound, *Liq. Cryst.*, 2022, **49**, 1784–1796.
8 S. Brown, E. Cruickshank, J. M. D. Storey, C. T. Imrie, D. Pociecha, M. Majewska, A. Makal and E. Gorecka, Multiple Polar and Non-polar Nematic Phases, *ChemPhysChem*, 2021, **22**, 2506–2510.
9 H. Nishikawa, K. Sano and F. Araoka, Anisotropic fluid with phototunable dielectric permittivity, *Nat. Commun.*, 2022, **13**, 1142.
10 R. J. Mandle, N. Sebastián, J. Martinez-Perdiguero and A. Mertelj, On the molecular origins of the ferroelectric splay nematic phase, *Nat. Commun.*, 2021, **12**, 4962.
11 A. Manabe, M. Bremer and M. Kraska, Ferroelectric nematic phase at and below room temperature, *Liq. Cryst.*, 2021, **48**, 1079–1086.
12 N. Vaupotič, D. Pociecha, P. Rybak, J. Matraszek, M. Čepič, J. M. Wolska and E. Gorecka, Dielectric response of a ferroelectric nematic liquid crystalline phase in thin cells, *Liq. Cryst.*, 2023, **50**, 584–595.
13 J. Szydlowska, P. Majewski, M. Čepič, N. Vaupotič, P. Rybak, C. T. Imrie, R. Walker, E. Cruickshank, J. M. D. Storey,

P. Damian and E. Gorecka, Ferroelectric Nematic–Isotropic Liquid Critical End Point, *Phys. Rev. Lett.*, 2023, **130**, 216802.
14 J. Li, R. Xia, H. Xu, J. Yang, X. Zhang, J. Kougo, H. Lei, S. Dai, H. Huang, G. Zhang, F. Cen, Y. Jiang, S. Aya and M. Huang, How Far Can We Push the Rigid Oligomers/Polymers toward Ferroelectric Nematic Liquid Crystals?, *J. Am. Chem. Soc.*, 2021, **143**, 46.
15 H. Nishikawa and F. Araoka, A New Class of Chiral Nematic Phase with Helical Polar Order, *Adv. Mater.*, 2021, **33**, 2101305.
16 N. Sebastián, L. Cmok, R. J. Mandle, M. R. De La Fuente, I. Drevenšek Olenik, M. Čopič and A. Mertelj, Ferroelectric–Ferroelastic Phase Transition in a Nematic Liquid Crystal, *Phys. Rev. Lett.*, 2020, **124**, 037801.
17 N. Sebastián, R. J. Mandle, A. Petelin, A. Eremin and A. Mertelj, Electrooptics of mm-scale polar domains in the ferroelectric nematic phase, *Liq. Cryst.*, 2021, **48**, 2055–2071.
18 Y. Song, M. Deng, Z. Wang, J. Li, H. Lei, Z. Wan, R. Xia, S. Aya and M. Huang, Emerging Ferroelectric Uniaxial Lamellar (Smectic AF) Fluids for Bistable In-Plane Polarization Memory, *J. Phys. Chem. Lett.*, 2022, **13**, 9983–9990.
19 C. Feng, R. Saha, E. Korblova, D. Walba, S. N. Sprunt, A. Jákli, C. Feng, S. N. Sprunt, A. Jákli, R. Saha, E. Korblova and D. Walba, Electrically Tunable Reflection Color of Chiral Ferroelectric Nematic Liquid Crystals, *Adv. Opt. Mater.*, 2021, **9**, 2101230.
20 N. Tufaha, E. Cruickshank, D. Pociecha, E. Gorecka, J. M. D. Storey and C. T. Imrie, Molecular Shape, Electronic Factors and the Ferroelectric Nematic Phase, *Chem. – Eur. J.*, 2023, **29**, e202300073.
21 S. Abe, Y. Shibata, M. Kimura and T. Akahane, Self-Consistent Explanation of the Untwist Alignment of Ferroelectric Nematic Liquid Crystals with Decreasing Cell Thickness and Deviation of the Surface Easy Axis Experimented upon Using the Brewster Angle Reflection Method, *Crystals*, 2024, **14**, 157.
22 H. Kamifuji, K. Nakajima, Y. Tsukamoto, M. Ozaki and H. Kikuchi, Effect of rubbing symmetry on polarization distribution in ferroelectric nematic liquid crystal cells, *Appl. Phys. Express*, 2023, **16**, 071003.
23 F. Ye, C. Yang, X. Zhang, X. Huang, Y. Zhu, S. Aya and M. Huang, High-κ elastomer with dispersed ferroelectric nematic liquid crystal microdroplets, *J. Mater. Chem. C*, 2024, **12**, 2738–2744.
24 C. L. Folcia, J. Ortega, R. Vidal, T. Sierra and J. Etxebarria, The ferroelectric nematic phase: an optimum liquid crystal candidate for nonlinear optics, *Liq. Cryst.*, 2022, **49**, 899–906.
25 J. Ortega, C. L. Folcia, J. Etxebarria and T. Sierra, Ferroelectric chiral nematic liquid crystals: new photonic materials with multiple bandgaps controllable by low electric fields, *Liq. Cryst.*, 2022, **49**, 2128–2136.
26 D. Pociecha, R. Walker, E. Cruickshank, J. Szydlowska, P. Rybak, A. Makal, J. Matraszek, J. M. Wolska, J. M. D. Storey, C. T. Imrie and E. Gorecka, Intrinsically chiral ferronematic liquid crystals: an inversion of the helical twist sense at the chiral nematic – chiral ferronematic phase transition, *J. Mol. Liq.*, 2021, **361**, 119532.
27 E. Zavvou, M. Klasen-Memmer, A. Manabe, M. Bremer and A. Eremin, Polarisation-driven magneto-optical and nonlinear-optical behaviour of a room-temperature ferroelectric nematic phase, *Soft Matter*, 2022, **18**, 8804–8812.
28 H. Nishikawa, K. Sano, S. Kurihara, G. Watanabe, A. Nihonyanagi, B. Dhara and F. Araoka, Nano-clustering mediates phase transitions in a diastereomerically-stabilized ferroelectric nematic system, *Commun. Mater.*, 2022, **3**, 89.
29 X. Chen, E. Korblova, M. A. Glaser, J. E. MacLennan, D. M. Walba and N. A. Clark, Polar in-plane surface orientation of a ferroelectric nematic liquid crystal: polar monodomains and twisted state electro-optics, *Proc. Natl. Acad. Sci. U. S. A.*, 2021, **118**, e2104092118.
30 J. Li, H. Nishikawa, J. Kougo, J. Zhou, S. Dai, W. Tang, X. Zhao, Y. Hisai, M. Huang and S. Aya, Development of ferroelectric nematic fluids with giant-dielectricity and nonlinear optical properties, *Sci. Adv.*, 2021, **7**, eabf5047.
31 A. Erkoreka, J. Martinez-Perdiguero, R. J. Mandle, A. Mertelj and N. Sebastián, Dielectric spectroscopy of a ferroelectric nematic liquid crystal and the effect of the sample thickness, *J. Mol. Liq.*, 2023, **387**, 122566.
32 N. A. Clark, X. Chen, J. E. MacLennan and M. A. Glaser, Dielectric spectroscopy of ferroelectric nematic liquid crystals: measuring the capacitance of insulating interfacial layers, *Phys. Rev. Res.*, 2024, **6**, 013195.
33 N. Yadav, Y. P. Panarin, W. Jiang, G. H. Mehl and J. K. Vij, Spontaneous mirror symmetry breaking and chiral segregation in the achiral ferronematic compound DIO, *Phys. Chem. Chem. Phys.*, 2023, **25**, 9083–9091.
34 G. W. Gray, K. J. Harrison and J. A. Nash, New family of nematic liquid crystals for displays, *Electron. Lett.*, 1973, **9**, 130–131.
35 J. Zhou, R. Xia, M. Huang and S. Aya, Stereoisomer effect on ferroelectric nematics: stabilization and phase behavior diversification, *J. Mater. Chem. C*, 2022, **10**, 8762–8766.
36 E. Cruickshank, R. Walker, J. M. D. Storey and C. T. Imrie, The effect of a lateral alkyloxy chain on the ferroelectric nematic phase, *RSC Adv.*, 2022, **12**, 29482–29490.
37 H. Kikuchi, H. Matsukizono, K. Iwamatsu, S. Endo, S. Anan and Y. Okumura, Fluid Layered Ferroelectrics with Global $C_{\infty v}$ Symmetry, *Adv. Sci.*, 2022, **9**, 2202048.
38 R. J. Mandle, A new order of liquids: polar order in nematic liquid crystals, *Soft Matter*, 2022, **18**, 5014–5020.
39 N. Sebastián, M. Čopič and A. Mertelj, Ferroelectric nematic liquid-crystalline phases, *Phys. Rev. E*, 2022, **106**, 021001.
40 Y. Song, J. Li, R. Xia, H. Xu, X. Zhang, H. Lei, W. Peng, S. Dai, S. Aya and M. Huang, Development of emergent ferroelectric nematic liquid crystals with highly fluorinated and rigid mesogens, *Phys. Chem. Chem. Phys.*, 2022, **24**, 11536–11543.
41 E. Cruickshank, A. Pearson, S. Brown, J. M. D. Storey, C. T. Imrie and R. Walker, The ferroelectric nematic phase: on the role of lateral alkyloxy chains, *Liq. Cryst.*, 2023, **50**, 1960–1967.
42 R. J. Mandle, S. J. Cowling and J. W. Goodby, Rational Design of Rod-Like Liquid Crystals Exhibiting Two Nematic Phases, *Chem. – Eur. J.*, 2017, **23**, 14554–14562.

43 E. Cruickshank, The Emergence of a Polar Nematic Phase: A Chemist's Insight into the Ferroelectric Nematic Phase, *ChemPlusChem*, 2024, e202300726.
44 P. Nacke, A. Manabe, M. Klasen-Memmer, X. Chen, V. Martinez, G. Freychet, M. Zhernenkov, J. E. Maclennan, N. A. Clark, M. Bremer and F. Giesselmann, New examples of ferroelectric nematic materials showing evidence for the antiferroelectric smectic-Z phase, *Sci. Rep.*, 2024, **14**, 1–13.
45 H. Nishikawa, F. Araoka, D. Stéfani Teodoro Martinez, R. Furlan de Oliveira, H. Nishikawa, M. Kuwayama, A. Nihonyanagi and B. Dhara, Rapid, solvent-minimized and sustainable access to various types of ferroelectric–fluid molecules by harnessing mechano-chemical technology, *J. Mater. Chem. C*, 2023, **11**, 12525–12542.
46 E. Cruickshank, N. Tufaha, R. Walker, S. Brown, E. Gorecka, D. Pociecha, J. M. D. Storey and C. T. Imrie, The influence of molecular shape and electronic properties on the formation of the ferroelectric nematic phase, *Liq. Cryst.*, 2024, **51**, 401–415.
47 E. Cruickshank, P. Rybak, M. M. Majewska, S. Ramsay, C. Wang, C. Zhu, R. Walker, J. M. D. Storey, C. T. Imrie, E. Gorecka and D. Pociecha, To Be or Not To Be Polar: The Ferroelectric and Antiferroelectric Nematic Phases, *ACS Omega*, 2023, **8**, 36562–36568.
48 M. Cigl, N. Podoliak, T. Landovský, D. Repček, P. Kužel and V. Novotná, Giant permittivity in dimethylamino-terminated ferroelectric nematogens, *J. Mol. Liq.*, 2023, **385**, 122360.
49 C. J. Gibb and R. J. Mandle, New RM734-like fluid ferroelectrics enabled through a simplified protecting group free synthesis, *J. Mater. Chem. C*, 2023, **11**, 16982–16991.
50 J. Karcz, N. Rychłowicz, M. Czarnecka, A. Kocot, J. Herman and P. Kula, Enantiotropic ferroelectric nematic phase in a single compound, *Chem. Commun.*, 2023, **59**, 14807–14810.
51 G. Stepanafas, E. Cruickshank, S. Brown, M. M. Majewska, D. Pociecha, E. Gorecka, J. M. D. Storey and C. T. Imrie, Ferroelectric nematogens containing a methylthio group, *Mater. Adv.*, 2023, **5**, 525–538.
52 X. Zhao, J. Zhou, J. Li, J. Kougo, Z. Wan, M. Huang and S. Aya, Spontaneous helielectric nematic liquid crystals: electric analog to helimagnets, *Proc. Natl. Acad. Sci. U. S. A.*, 2021, **118**, e2111101118.
53 X. Chen, V. Martinez, P. Nacke, E. Korblova, A. Manabe, M. Klasen-Memmer, G. Freychet, M. Zhernenkov, M. A. Glaser, L. Radzihovsky, J. E. Maclennan, D. M. Walba, M. Bremer, F. Giesselmann, N. A. Clark, N. Abbott and P. Palffy-Muhoray, Observation of a uniaxial ferroelectric smectic A phase, *Proc. Natl. Acad. Sci. U. S. A.*, 2022, **119**, e2210062119.
54 S. Nishimura, S. Masuyama, G. Shimizu, C.-Y. Chen, T. Ichibayashi and J. Watanabe, Lowering of Electrostatic Actuator Driving Voltage and Increasing Generated Force Using Spontaneous Polarization of Ferroelectric Nematic Liquid Crystals, *Adv. Phys. Res.*, 2022, **1**, 2200017.
55 H. Matsukizono, K. Iwamatsu, S. Endo, Y. Okumura, S. Anan and H. Kikuchi, Synthesis of liquid crystals bearing 1,3-dioxane structures and characterization of their ferroelectricity in the nematic phase, *J. Mater. Chem. C*, 2023, **11**, 6183–6190.
56 A. A. Marchenko, O. L. Kapitanchuk, Y. Y. Lopatina, K. G. Nazarenko, A. I. Senenko, N. Katsonis, V. G. Nazarenko and O. D. Lavrentovich, Polar Self-Organization of Ferroelectric Nematic-Liquid-Crystal Molecules on Atomically Flat Au(111) Surface, *Phys. Rev. Lett.*, 2024, **132**, 098101.
57 N. V. Madhusudana, Simple molecular model for ferroelectric nematic liquid crystals exhibited by small rodlike mesogens, *Phys. Rev. E*, 2021, **104**, 014704.
58 R. J. Mandle, Implementation of a cylindrical distribution function for the analysis of anisotropic molecular dynamics simulations, *PLoS One*, 2022, **17**, e0279679.
59 R. J. Mandle, In Silico Interactome of a Room-Temperature Ferroelectric Nematic Material, *Crystals*, 2023, **13**, 857.
60 A. Zattarin, E. Cruickshank, D. Pociecha, J. M. D. Storey, E. Gorecka and C. T. Imrie, A design approach to obtaining highly polar liquid crystal dimers, *Liq. Cryst.*, 2024, **51**, 1035–1046.
61 M. J. Frisch, G. W. Trucks, H. B. Schlegel, G. E. Scuseria, M. A. Robb, J. R. Cheeseman, G. Scalmani, V. Barone, B. Mennucci, G. A. Petersson, H. Nakatsuji, M. Caricato, X. Li, H. P. Hratchian, A. F. Izmaylov, J. Bloino, G. Zheng, J. L. Sonnenberg, M. Hada, M. Ehara, K. Toyota, R. Fukuda, J. Hasegawa, M. Ishida, T. Nakajima, Y. Honda, O. Kitao, H. Nakai, T. Vreven, J. A. Montgomery, J. E. Peralta, F. Ogliaro, M. Bearpark, J. J. Heyd, E. Brothers, K. N. Kudin, V. N. Staroverov, R. Kobayashi, J. Normand, K. Raghavachari, A. Rendell, J. C. Burant, S. S. Iyengar, J. Tomasi, M. Cossi, N. Rega, J. M. Millam, M. Klene, J. E. Knox, J. B. Cross, V. Bakken, C. Adamo, J. Jaramillo, R. Gomperts, R. E. Stratmann, O. Yazyev, A. J. Austin, R. Cammi, C. Pomelli, J. W. Ochterski, R. L. Martin, K. Morokuma, V. G. Zakrzewski, G. A. Voth, P. Salvador, J. J. Dannenberg, S. Dapprich, A. D. Daniels, O. Farkas, J. B. Foresman, J. V. Ortiz, J. Cioslowski and D. J. Fox, *Gaussian 09, Revision B.01*, Gaussian, Inc., Wallingford CT, 2010.
62 M. Tarini, P. Cignoni and C. Montani, Ambient occlusion and edge cueing to enhance real time molecular visualization, *IEEE Trans. Vis. Comput. Graphics*, 2006, **12**, 1237–1244.
63 X. Chen, V. Martinez, E. Korblova, G. Freychet, M. Zhernenkov, M. A. Glaser, C. Wang, C. Zhu, L. Radzihovsky, J. E. Maclennan, D. M. Walba and N. A. Clark, The smectic ZA phase: antiferroelectric smectic order as a prelude to the ferroelectric nematic, *Proc. Natl. Acad. Sci. U. S. A.*, 2022, **120**, e2217150120.
64 A. V. Emelyanenko, V. Y. Rudyak, S. A. Shvetsov, F. Araoka, H. Nishikawa and K. Ishikawa, Emergence of paraelectric, improper antiferroelectric, and proper ferroelectric nematic phases in a liquid crystal composed of polar molecules, *Phys. Rev. E*, 2022, **105**, 064701.
65 M. Mrukiewicz, M. Czerwiński, N. Podoliak, D. Repček, P. Perkowski, R. J. Mandle and D. Węgłowska, Polar nematic phases with enantiotropic ferro- and antiferroelectric behaviour, *J. Mater. Chem. C*, 2024, **12**, 7214–7224.
66 T. Donaldson, H. Staesche, Z. B. Lu, P. A. Henderson, M. F. Achard and C. T. Imrie, Symmetric and non-symmetric chiral liquid crystal dimers, *Liq. Cryst.*, 2010, **37**, 1097–1110.

67 V. Matko, E. Gorecka, D. Pociecha, J. Matraszek and N. Vaupotič, Interpretation of dielectric spectroscopy measurements of ferroelectric nematic liquid crystals, *Phys. Rev. Res.*, 2024, **6**, L042017.
68 N. Yadav, Y. P. Panarin, J. K. Vij, W. Jiang and G. H. Mehl, Two mechanisms for the formation of the ferronematic phase studied by dielectric spectroscopy, *J. Mol. Liq.*, 2023, **378**, 121570.
69 A. Erkoreka and J. Martinez-Perdiguero, Constraining the value of the dielectric constant of the ferroelectric nematic phase, *Phys. Rev. E*, 2024, **110**, L022701.
70 A. Adaka, M. Rajabi, N. Haputhantrige, S. Sprunt, O. D. Lavrentovich and A. Jákli, Dielectric properties of a ferroelectric nematic material: quantitative test of the polarization-capacitance Goldstone mode, *Phys. Rev. Lett.*, 2024, **133**, 038101.